

Investigation of the Interactions and Bonding between Carbon and Group VIII Metals at the Atomic Scale

Thilo Zoberbier, Thomas W. Chamberlain, Johannes Biskupek, Mikhail Suyetin, Alexander G. Majouga, Elena Besley, Ute Kaiser,* and Andrei N. Khlobystov*

The nature and dynamics of bonding between Fe, Ru, Os, and single-walled carbon nanotubes (SWNTs) is studied by aberration-corrected high-resolution transmission electron microscopy (AC-HRTEM). The metals catalyze a wide variety of different transformations ranging from ejection of carbon atoms from the nanotube sidewall to the formation of hollow carbon shells or metal carbide within the SWNT, depending on the nature of the metal. The electron beam of AC-HRTEM serves the dual purpose of providing energy to the specimen and simultaneously enabling imaging of chemical transformations. Careful control of the electron beam parameters, energy, flux, and dose allowed direct comparison between the metals, demonstrating that their chemical reactions with SWNTs are determined by a balance between the cohesive energy of the metal particles and the strength of the metal–carbon σ - or π -bonds. The pathways of transformations of a given metal can be drastically changed by applying different electron energies (80, 40, or 20 keV), thus demonstrating AC-HRTEM as a new tool to direct and study chemical reactions. The understanding of interactions and bonding between SWNT and metals revealed by AC-HRTEM at the atomic level has important implications for nanotube-based electronic devices and catalysis.

T. Zoberbier, Dr. J. Biskupek, Prof. U. Kaiser
Central Facility for Electron Microscopy
Electron Microscopy Group of Materials Science
Ulm University
Albert-Einstein-Allee 11, Ulm D-89081, Germany
E-mail: ute.kaiser@uni-ulm.de

Dr. T. W. Chamberlain
Institute of Process Research and Development
School of Chemistry
University of Leeds
Leeds LS2 9JT, United Kingdom

Dr. T. W. Chamberlain, Dr. M. Suyetin,^[+]

Prof. E. Besley, Prof. A. N. Khlobystov
School of Chemistry
University of Nottingham
University Park

Nottingham NG7 2RD, United Kingdom
E-mail: andrei.khlobystov@nottingham.ac.uk

Prof. A. G. Majouga, Prof. A. N. Khlobystov
National University of Science & Technology MISiS
Moscow 119049, Russia

^[+]Present address: Physical Sciences and Engineering, King Abdullah
University of Science & Technology, Thuwal, Makkah 23955, Saudi Arabia

DOI: 10.1002/sml.201502210



1. Introduction

In order to unlock the full potential of carbon nanostructures (nanotubes, fullerenes, and graphene) the understanding of their bonding and interactions with different metals is becoming increasingly important on two different levels. First is the need to control the formation processes of carbon nanostructures which are often catalyzed and templated by transition metals. The second is the harnessing of their functional properties which relies on the interface with metallic contacts in electronic devices, such as field-effect transistors, or interactions with metal nanoparticles in fuel cells and other catalytic materials. Metal–carbon bonding lies at the core of all these important quests and holds the key to development of technologies based on carbon nanostructures.

Metal–graphene and metal–nanotube interactions have been the subject of several theoretical studies. Bonding between the π -electronic system of nanotubes or graphene and metal atoms (referred to as π -bonding) is expected to consist of covalent and ionic components and have a typical bonding energy in the range of 0–2 eV, depending on the nature of the metal and the curvature of the carbon nanostructure (e.g., cylindrical nanotube vs planar graphene).^[1–6]

A theoretical comparison of different transition metals reveals a nonuniform dependence of the π -bonding energy within the period of the 3d-elements, which can be described as a double-maxima dependence on the atomic number.^[1,7] Interestingly, graphene and nanotube surfaces exhibit qualitatively similar trends of π -bonding with 3d-metal atoms which appear to extend to continuous metallic surfaces.^[1,8,9]

Carbon nanostructures often incorporate different types of structural defects which significantly alter their properties. Even the simplest of defects – a single-vacancy (SV, when a carbon atom is removed from the graphene or nanotube lattice) – drastically changes the bonding of metals with nanotubes or with graphene.^[3,4,10–14] Metal atoms have been shown to form σ -bonds with radicals localized around defects which increases the covalent component and thus the bonding energy of the interaction. The energy of such σ -bonding has been explored in detail for 3d-metals and exhibits a two-maxima trend along the period^[10,13,14] similar to that observed for π -bonding. No systematic analysis has yet been performed for 4d- and 5d-metals, which are as important for the synthesis and applications of nanotubes and graphene as 3d-metals. Additionally, theoretical studies of trends within groups of the periodic table are limited to Group-XI (coinage metals), thus leaving wide scope for future theoretical investigations.^[3]

Recent developments in transmission electron microscopy (TEM) have made this method highly significant, being the most direct way of studying interactions between transition metals and carbon nanostructures at the atomic level. The spatial resolution of TEM is sufficiently high for direct-space visualization of isolated metal atoms on graphene or nanotubes, and the external parameters, such as the energy of the electron beam (e-beam), temperature, and local environment can be precisely controlled, so that their impact on the metal–carbon bonding can be studied in detail at the atomic level. The relatively low energy of π -bonding results in high diffusivity of metal atoms (e.g., tens of μm for Au on graphene) making it difficult to pinpoint the positions of individual atoms and to study their interactions with graphene or carbon nanotubes.^[15–21] This essentially unrestricted diffusion of metal atoms on carbon surfaces leads to aggregation of metals into clusters which is driven by the cohesive energy of the metal, outweighing the metal–carbon π -bonding,^[16,17,19,20] with an exception of a recent example where graphene is doped with heteroatoms.^[22] Therefore, the relative bonding energies for different metals can be inferred from the homogeneity of metal distribution on nanotube surfaces or, most recently, from the direct observation of individual metal atoms on graphene by aberration corrected scanning TEM utilizing a 60 keV e-beam.^[17,19] Currently available experimental observations for different metals appear to be in line with the theoretically predicted trends of π -bonding.^[17,19]

When the energy of the e-beam is significantly above the threshold required for the removal of C-atoms from a nanotube or graphene, vacancy defects can be purposefully created by the e-beam.^[15,23,24] As defect sites provide significantly stronger σ -bonding, they act as traps for transition metals. Observation of the escape processes of metal atoms from such vacancy-traps at different temperatures allows estimation of the energy of metal–carbon σ -bonding.^[15,18] It is interesting

that some transition metals facilitate the formation of defects in graphene by the e-beam, even when the energy of the e-beam is insufficient for direct removal of carbon atoms.^[16,19] Transition metals and their clusters are expected to stabilize vacancy defects in graphene, but the exact mechanism of this process is complex^[25] and not fully understood.^[12] As the defect increases in size, metal atoms diffuse toward the edge and form σ -bonds with the outermost carbon atoms which can stabilize the highly reactive carbon radicals.^[16,26]

Several recent breakthroughs have shed light on the complexity of interactions between metals and carbon nanostructures.^[27,28] A number of detailed systematic theoretical studies focused on 3d-metals and investigated trends within the period, leaving 4d- and 5d-metals and trends within the groups of the periodic table largely unexplored. In contrast to the theoretical works, current experimental studies are significantly less systematic and usually report sporadic examples for metals from different places of the periodic table, which nevertheless provide some valuable information and can be effectively correlated with theoretical predictions.^[1–14] Systematic experimental measurements on a series of related metals are hampered by technical difficulties associated with deposition of transition metals on graphene or nanotube surfaces. In this study, we employ single-walled carbon nanotubes (SWNTs) as containers for three group VIII metals (Fe, Ru, and Os), which have the same number of valence electrons but belong to three different periods representing 3d-, 4d-, and 5d-metals. Confinement of the metals in the tiny channels of SWNTs overcomes most of the challenges highlighted in previous reports (e.g., oxidation of the metal, aggregation of the metal into large clusters, fast unrestricted diffusion of metal atoms, and any interference by surface contamination). Recently our methodology has been successfully employed for a comparative study of metal–nanotube bonding for neighbouring metals from the same period.^[26] Herein, we report the first comparative study for metals belonging to the same group of the periodic table revealing the richness of chemical transformations promoted by d-metals of different periods.

2. Results and Discussion

2.1. Methodology

The imaging electron-beam used in aberration corrected TEM (AC-TEM) has multiple effects on the specimen manifested as kinetic energy transferred to individual atoms, ionization (due to inelastic collisions with atoms), heating and/or generation of free radicals (due to homolysis of chemical bonds). SWNT structures possess unique properties which effectively minimize several of the detrimental effects of the e-beam on the specimen. SWNTs are very thin and possess extremely high thermal and electronic conductance, thus mitigating any heating and ionization effects and act as effective shields for molecules and atoms encapsulated within nanotubes.^[29] This is because guest molecules forming intimate contact with the nanotube sidewalls are interacting with the infinite pool of delocalized electrons of the SWNT. The quasi-free π -electrons

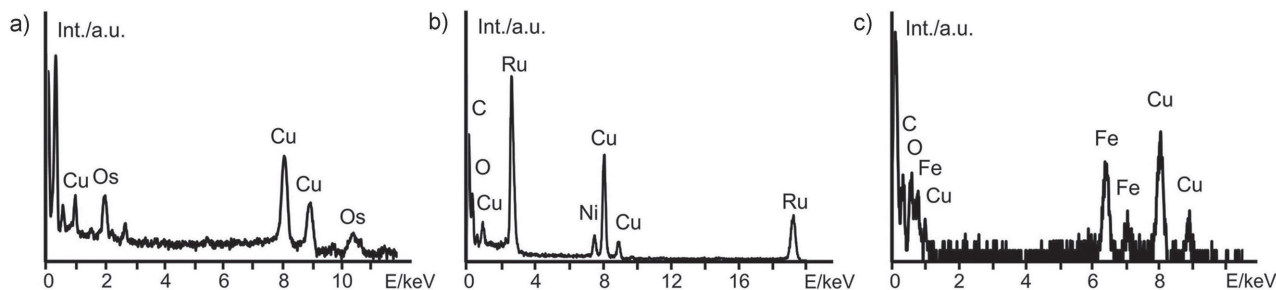


Figure 1. EDX spectra recorded at 100 keV primary electron energy and integrated over a small bundle of nanotubes confirms the presence of the different transition metals inside SWNT: a) Osmium, b) ruthenium, and c) iron sample. Cu peaks are due to the specimen TEM grid, and Ni peaks are due to residual nanotube growth catalyst outside nanotubes.

of the host-nanotube can be withdrawn on a much shorter timescale than any changes in interatomic bonding induced by the e-beam can occur. As a result metal nanoparticles encapsulated in SWNTs are largely protected from ionization or heating. Being chemically very stable, carbon nanotubes also protect guest-species from any free radicals or other reactive organic fragments generated by the e-beam.

The direct displacement of carbon atoms of the nanotube due to the kinetic energy transfer of incident electrons is precluded by reducing the energy of the e-beam to below 80 keV in all of our experiments. In this regime the probability for knock-on damage is negligible (Supporting Information) and therefore nearly all structural transformations observed on the time scale of our experiments were due to nanotube-metal interactions, ultimately defined by the chemical properties of the element encapsulated in the nanotube.^[23,30] However, as any nanotube contains some structural defects, such as mono-vacancies, which will have a greater susceptibility to e-beam damage (Supporting Information), we selected SWNTs synthesised by electric arc discharge as they possess fewer defects than nanotubes produced by other methods, and for the time-series imaging of metal clusters we chose sections of SWNT that were largely defect-free at the start of imaging. As the rates of chemical transformations are highly dependent on the energy and dose of the e-beam, the dose was also carefully controlled in our experiments. We imaged the evolution of metal clusters and their interactions with carbon continuously using an electron flux between 10^6 – 10^7 $e^- \text{ nm}^{-2} \text{ s}^{-1}$ and a cumulative dose for each image series of $\approx 10^{10}$ $e^- \text{ nm}^{-2}$. Our time series imaging demonstrates that under such experimental conditions any pre-existing defects in metal-free SWNT evolve significantly slower than in the presence of a transition metal. Therefore, by comparing time series of images for different metals recorded under the same TEM conditions, we can draw conclusions about the nature and energy of the metal-nanotube interactions and the bonding for each element in the Group-VIII of the periodic table.

2.2. Observations

The transition metals Fe, Ru, and Os were encapsulated in carbon nanotubes in the form of metal carbonyls $M_x(\text{CO})_y$, which can be easily broken down into pure metal and CO gas.^[31] While metals aggregate into clusters of 50–100 atoms

forming intimate contact with the nanotube inner (concave) surface (see the figures below), carbon monoxide vents out of the nanotubes. The identities of metallic clusters formed in nanotubes are confirmed by energy dispersive X-ray (EDX) spectroscopy using a focused 100 keV electron beam irradiating a small bundle of 5–10 filled SWNTs (**Figure 1**). In contrast to several methods developed for insertion of metallic particles into multiwalled carbon nanotubes, no practical method existed for single-walled nanotubes until recently.^[31] Our approach offers a simple, clean, and reproducible method that can be applied effectively for a wide range of metals, including the Group-VIII metals Fe, Ru, and Os.

The electron beam in our experiments served a dual purpose: it is the imaging tool and at the same time a source of energy promoting chemical transformations in the observed area of the specimen. As the energy of the e-beam in all of our experiments (80, 40, or 20 keV) was below the onset value for direct removal of carbon atoms from a hexagonal carbon lattice, i.e., the SWNT sidewall, no measurable structural transformations take place on the timescale of our experiments in defect-free SWNTs without the presence of a metal.^[23,30] Particles of transition metal embedded within the carbon nanotube weaken the atomic structure of the SWNT to a certain, element-specific degree, making it possible to measurably remove carbon atoms from the sidewall even using an electron energy below 85 keV. Our detailed observations showed, depending on the nature of the transition metal, that it is possible for a carbon atom to become dislodged by the e-beam and leave the SWNT, thus undergoing a metal-assisted e-beam induced ejection (EBIE) (**Figure 2b**). Alternatively, the dislodged or otherwise activated carbon atom can remain within the nanotube and engage in bonding with the metal particle forming new carbon structures (**Figure 2a**), undergoing a process of metal-assisted e-beam induced restructuring (EBIR), akin to metal-catalyzed growth of carbon nanostructures such as nanotubes or graphene. Our measurements indicate that the exact behavior under a given set of conditions is defined by the physicochemical properties of the transition metal inside the nanotube.

Within the group VIII triad, Fe–Ru–Os, osmium has the highest cohesive energy (**Table 1**). As a consequence, Os clusters remain spheroidal and compact, with closed, partially faceted surfaces, during TEM observations at 80 keV (**Figure 3a**). Slow rotational motion allowed clear visualization of the hexagonal lattice (consistent with space group

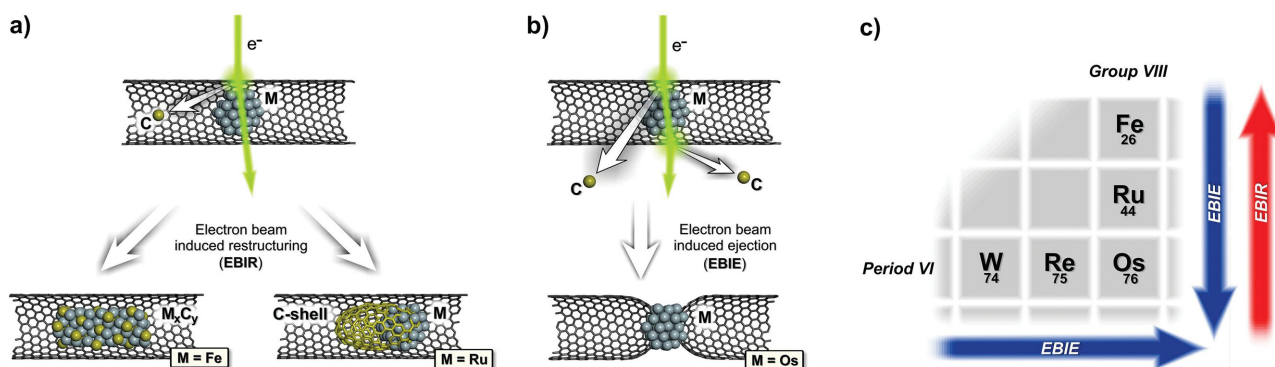


Figure 2. a) The electron-beam-induced restructuring process: initially a carbon atom from the SWNT sidewall in the vicinity of the metal cluster is dislodged by the e-beam. The dislodged C-atom adheres to the metal cluster and proceeds to form metal carbide (as in the case of Fe, left) or a carbon shell (as in the case of Ru, right). b) In the electron beam induced ejection process the, dislodged carbon atom is completely removed from the specimen, causing gradual development of sidewall defects and breakage of the nanotube (as in the case of Os). c) The role that EBIE and EBIR mechanisms play, increases in opposite directions within group VIII of the periodic table.

$P6_3/mmc$ of the bulk metal) of Os confirming the metallic nature of Os clusters. Osmium atoms are involved in the strongest interactions and bonding with the nanotubes concave surface. They facilitate the rapid formation of vacancy-type defects in SWNT sidewalls via the EBIE mechanism leading to covalent σ -bonding of Os with the edges of defects (Figure 3g). To compensate for the continuous loss of carbon atoms promoted by Os clusters, the nanotube undergoes extensive restructuring manifested in narrowing of the nanotube diameter (Figure 3h) and eventually complete breakage of the SWNT at an e-dose of $\approx 10^9$ e⁻ nm⁻². The observed behavior clearly indicates the high affinity of Os for carbon resulting in effective σ -bonding, which facilitates the formation of defects in the host-nanotube due to the ejection of C atoms from the specimen by the 80 keV e-beam. Our density functional theory (DFT) calculations confirm that within the group VIII elements, Os forms the strongest σ -bonds with carbon (Table 1), which are necessary for the formation of extensive sidewall defects in the host SWNT. Examples of EBIR processes for Os clusters are significantly rarer. Indeed, our previous comparative study of transition metals W–Re–Os along period 6 of the periodic table demonstrated that Os is most active toward the EBIE mechanism with no significant EBIR processes observed for any of the elements of this triad under the experimental conditions used in that study.^[26]

However, ascending in group VIII from Os to Ru showed marked changes in the observed behavior of the metal clusters. Under the same imaging conditions Ru clusters appear to have a more diffuse surface and much faster dynamics

than Os, continuously changing their shapes, so that exact determination of the metal atoms positions was challenging for this metal (Figure 4a), which reflects the lower cohesive energy of Ru (Table 1). HRTEM contrast of Ru clusters and measured interatomic distances suggest that the ruthenium remains metallic within the nanotubes. Ru clusters facilitate the formation of sidewall defects of very limited size and to a significantly lower extent than for Os clusters, with the result that no breakage of the SWNT can be caused. No significant EBIE-type activity occurred, even during extended e-beam exposure, with many more EBIR transformations observed for ruthenium: the metal clusters appear to collect carbon atoms around them, in most cases forming spheroidal carbon shells (Figure 4d–i). Such carbon shells, structurally similar to fullerenes, were found to be attached by their open side to the Ru clusters, (Figure 4d–i) thus blocking most of the metal atoms from interactions with the host SWNT. In some cases carbon shells were found to wrap around the Ru cluster, completely enveloping it (Figure 4d). Due to their very high curvature, the shells formed on Ru are metastable in the 80 keV e-beam and undergo further transformations opening up and allowing limited interactions between the ruthenium atoms and the inner side of the SWNT (Figure 4g–i). Nevertheless, their presence definitely inhibits any direct reactions between the metal and the nanotube.

Instead of facilitating the process of carbon atom ejection by the EBIE mechanism, as in the case of osmium, ruthenium engages in more diverse bonding with carbon and plays the role of template promoting the assembly of new carbon nanostructures via a mechanism similar to that proposed for

Table 1. Physicochemical parameters of group VIII metals determining their reactivity with carbon nanotubes under the electron beam.

Metal	Cohesive energy ^[32] [kJ mol ⁻¹]	M–C σ -bond energy ^{a)} [kJ mol ⁻¹]	M–C π -bond energy ^{b)} [kJ mol ⁻¹]	Stable carbide ^[33]
Os	1713	1040	84	No
Ru	1142	898	160	No
Fe	898	802	90	Yes

^{a)}Calculated for σ -bonding of corresponding metal atoms with a tetra-vacancy defect in a SWNT sidewall; binding energies for mono- and di-vacancy follow the same trend of relative energies;

^{b)}Calculated for the concave side of a carbon nanotube.

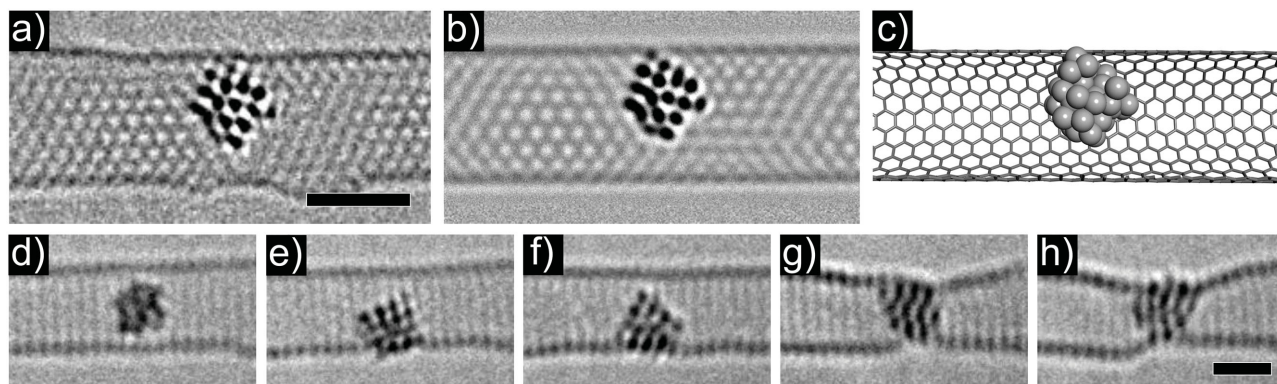


Figure 3. 80 keV AC-HRTEM investigations of the group VIII metal Os inside SWNTs. a–c) The strong correlation between experiment and simulation supports that Os forms compact clusters with faceted shape and metallic structure as displayed in the a) AC-HRTEM close-up image, b) corresponding image simulation, and c) structure model. d–h) Additional time-series snapshots show a cluster of Os interacting with the SWNT sidewall via the EBIE process finally resulting in constriction of the nanotube. Scale bars = 1 nm.

metal-catalyzed SWNT growth.^[34] The energy of the Ru–C σ -bond is lower than Os–C, as shown by our calculations, while the cohesive energy of Ru-clusters is significantly lower than Os (Table 1). Both these parameters stimulate a more dynamic behavior and the more diverse reactivity of ruthenium in nanotubes as compared to osmium. Interestingly, the calculated energy of a Ru–C π -bond is substantially higher than for other metals in the group VIII (Table 1), which may explain the observed propensity for the formation of carbon shells around Ru clusters maximizing the number of Ru–C π -bonds (Figure 4d–i). As the EBIR processes become more prevalent for Ru, they cause passivation of the cluster surface (by the carbon shell), which in turn suppresses the EBIE behavior of this metal (Figure 2b). These chemical processes observed by direct-space AC-high resolution TEM (AC-HRTEM) imaging are reminiscent of the well-known metal surface carburization which takes place in catalysis and significantly affects the properties of the transition metal catalysts.

Iron clusters were shown to undergo the most drastic transformation inside carbon nanotubes under the 80 keV e-beam and among the observed triad it is the only metal

which forms carbide compound clusters inside SWNTs. Some Fe clusters become elongated and their structures appear to remain unchanged over much longer periods of time exhibiting virtually no interactions with the host SWNT (Figure 5d–h). Precise assignment of specific iron carbide phases, which can appear similar in small quasi-crystals, is challenging because of surface effects and significant structural distortions, which may be further exacerbated by dynamic processes caused by the e-beam. However, detailed structural analysis and image simulation (Supporting Information) indicate that the observed iron carbide phase (Figure 5a,d–h) is most likely to be Fe_3C in the space group of symmetry $Pnma$. The fact that the surface of the Fe_3C clusters is typically separated from the nanotube sidewall by a van der Waals gap of 0.3 nm and that no significant interactions between SWNT and the cluster were observed even at doses of $8 \times 10^{10} \text{ e}^- \text{ nm}^{-2}$ indicate that the surface of the carbide is terminated with C atoms which preclude the direct metal–nanotube contact required for defect formation via the EBIE mechanism. The image simulation of $\text{Fe}_3\text{C}@$ SWNT (Figure 5b) further supports the presence of a

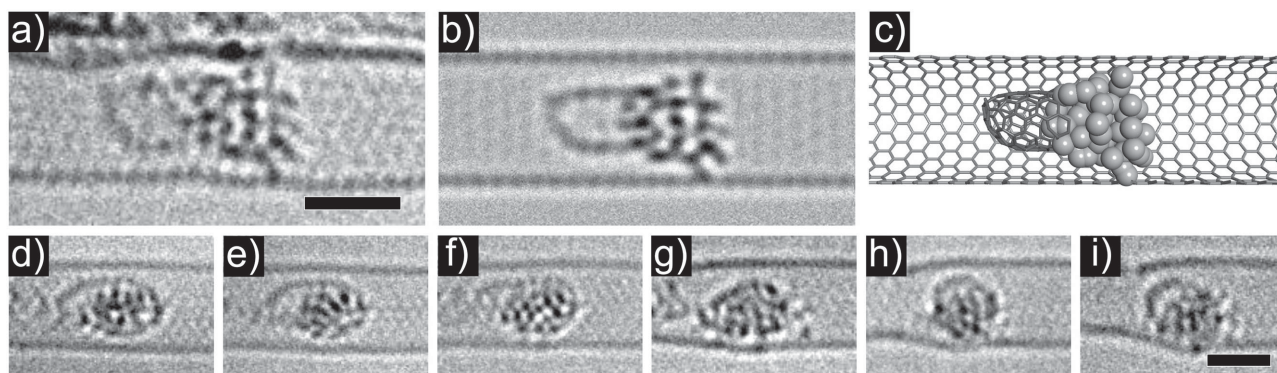


Figure 4. 80 keV AC-HRTEM investigations of the group VIII metal Ru inside SWNTs. a–c) The strong correlation between experiment and simulation suggests that Ru clusters have metallic nature with diffuse shape as shown in the a) close-up image, b) corresponding image simulation, and c) structure model. d–i) The clusters predominantly interact with carbon via the EBIR process manifested in shell formation and modification, d) the metastable shells enclose parts of the metal clusters but rarely envelope them completely, g–i) openings or defects in the shell allow some interactions with the host SWNT enabling Ru to extract carbon atoms from the nanotube and incorporate them into the carbon structure growing on the Ru (EBIR); while the SWNT develops a moderate defect after a significant dose of the e-beam in this case, the rate and extent of defect formation in EBIR is substantially lower than in EBIE under similar conditions. Scale bars = 1 nm.

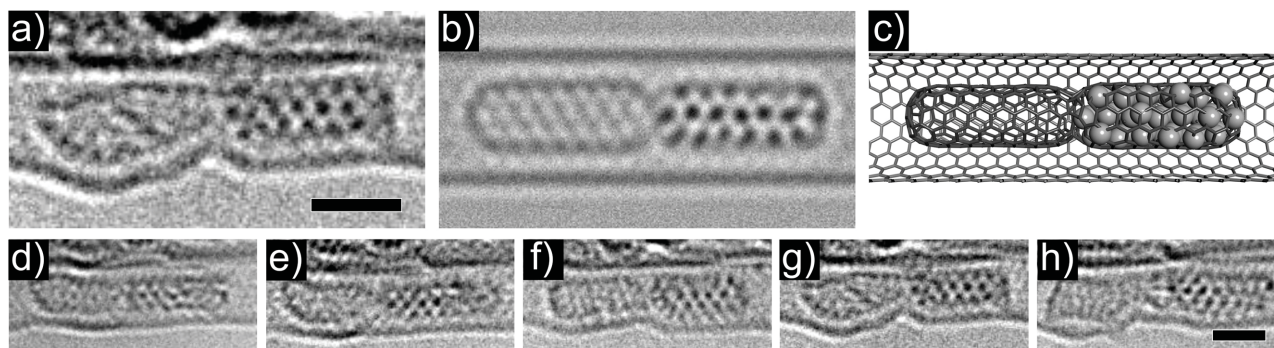


Figure 5. 80 keV AC-HRTEM investigations of the group VIII metal Fe in SWNTs. a–c) The strong correlation between experiment and simulation supports that clusters inside SWNTs exist in the iron-carbide phase with elongated carbon shells attached at their termini: a) AC-HRTEM image, b) corresponding image simulation based on Fe_3C with $Pnma$ structure, and c) the structure model. A range of typical transformations for iron observed under an 80 keV electron beam shown in panels (d–h): Fe forms slowly rotating, elongated Fe_3C particles which are separated by a van der Waals sized gap from the host SWNT. This confirms that the iron carbide cluster surface is terminated with C atoms stabilizing the cluster and preventing further interactions between Fe and the SWNT. f–g) Some carbon atoms are expected to be extracted from the SWNT by the metal to form the carbide, thus resulting in sidewall defects within the nanotube that after extensive exposure to the e-beam undergo transformations (distortions of the SWNT sidewall), which however have a significantly lower rate and extent as compared to EBIE under similar conditions. Scale bars = 1 nm.

layer of C atoms on the surface of the Fe_3C cluster, which is required to match the experimental HRTEM contrast. Most Fe_3C clusters also have carbon shells extruding from their termini (Figure 5a,d–h). The unique behavior of Fe, as compared to the other group VIII metals can be related to the fact that iron has the lowest cohesive energy and is the only metal in the triad that is able to form sufficiently stable carbides (Table 1). Once bound within a carbide compound, the Fe atoms are not able to interact with the nanotube sidewall as effectively as Os or Ru, so that any kind of EBIE activities are largely suppressed in the specimen, and the host-nanotube sidewalls remain essentially intact on the timescale of our experiments, as compared to Ru and particularly Os. The formation of a carbide compound can be viewed as the most extreme case of EBIR, as the metal and carbon atoms become intermixed on the atomic level within the iron carbide particle. Indeed, our AC-HRTEM observations demonstrate a remarkable link to the carburization of Fe in catalytic processes which often takes place in preparative catalysis and plays a significant role in important industrial reactions, such as Fischer–Tropsch synthesis.

The experimentally observed extent of transformations of metal clusters due to interactions and bonding with carbon (EBIR activity) decreases upon descending group VIII, $\text{Fe} > \text{Ru} > \text{Os}$, which is manifested in the formation of carbon cages around Ru and the transformation of Fe into iron carbide. This order correlates with the cohesive energy of metallic particles, explaining why it is more energetically favorable for Os to remain in the pure metallic form. The observed pathways of metal–carbon reactions are related to the chemical properties of the metals, such as the enhanced ability to form σ -bonds (as in the case of Os), π -bonds (as in the case of Ru) or the high stability of metal carbides (as in the case of Fe). As a result of these reactions, the reactivity of the transition metals of group VIII toward the SWNT sidewall (EBIE activity) becomes progressively passivated upon ascending the Group, $\text{Os} > \text{Ru} > \text{Fe}$. Profiles of the two competing processes (EBIR vs EBIE) based on multiple

HRTEM observations for these metals are schematically illustrated in **Figure 6**.

The comparative study of group VIII metals clearly demonstrates that the chemical properties of the elements encapsulated within nanotubes hold the key to control the reactivity of SWNTs. Another important parameter that has been shown to drastically change the structural transformations observed for a given metal is the energy of the e-beam. Our observations demonstrate that different types of behavior can be switched on and off for the same metal using incident electrons at different energies. For example, lowering the e-beam energy to 40 keV drastically alters the behavior of Os clusters from EBIE to EBIR (compare **Figure 7a** and **b**). Incident electrons at 40 keV are still able to promote dislodging of carbon atoms from the SWNT sidewall in the vicinity of Os clusters, but are not powerful enough to cause their complete ejection from the specimen (EBIE mechanism). As a result, at 40 keV the activated carbon atoms remain bound to Os and produce extended carbon shells, somewhat similar to those observed for Ru at 80 keV, but extending outward from the host SWNT and forming branched protrusions (Figure 7b). Formation of similar carbon protrusions under an 80 keV electron beam was previously reported for SWNT filled with ReC_{60} complexes.^[35] Further reduction of the e-beam energy to 20 keV showed much reduced EBIR activity with most Os clusters remaining inactive toward the nanotube (Figure 7c). Although atomic resolution at 20 or 40 keV cannot be currently achieved, comparative time series (Supporting Information) clearly indicates that the 20 keV e-beam is not sufficient to promote any significant metal-assisted transformation in the nanotube of either EBIE- or EBIR-type (**Table 2**).

3. Conclusions

Low-voltage AC-HRTEM imaging enables visualization of nanoscale structures and time-resolved transformations at

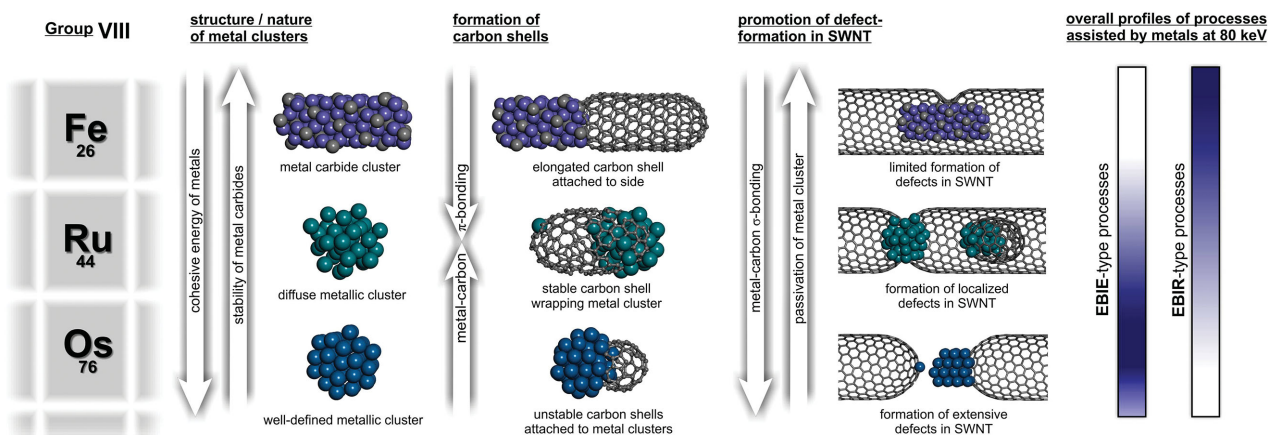


Figure 6. Schematic representation of the trends observed by 80 keV AC-HRTEM in group VIII metals inside SWNTs. The behavior of the metal clusters is determined by a balance of the physicochemical properties of the metals, including cohesive energy, stability of the carbide phases, and energies of M–C π - and σ -bonding. Overall, the EBIE processes increase and the EBIR processes decrease down the group VIII triad: Fe–Ru–Os.

the atomic level. Comparative study of the interactions and bonding of transition metals demonstrates that metals can be engaged in interactions with carbon nanotubes in different

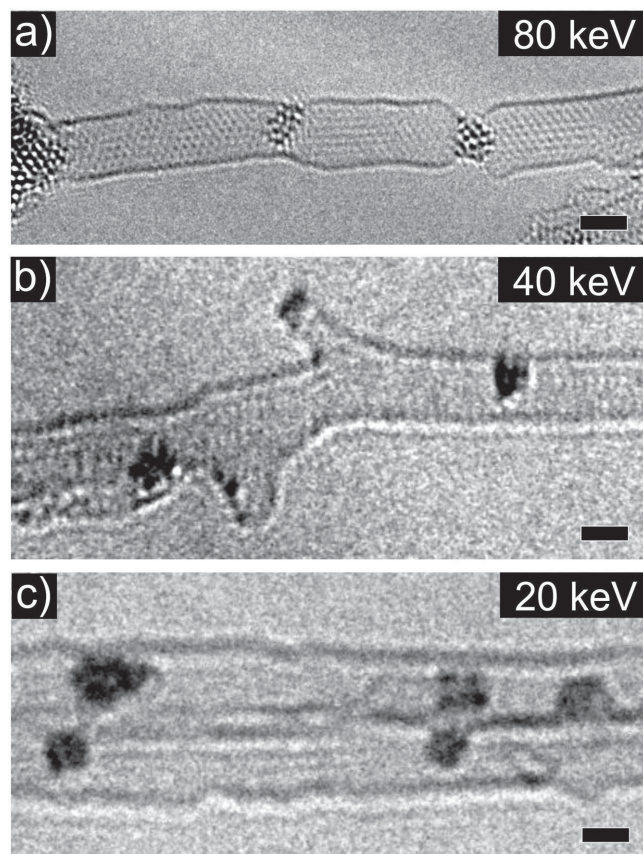


Figure 7. a) AC-HRTEM images at different e-beam energies for Os@SWNT show that at lower energies EBIR processes replace EBIE processes. At 80 keV Os facilitates ejection of C atoms from the host SWNT leading to extensive sidewall defects. b) At 40 keV Os restructures the nanotube locally forming elongated carbon nanoprotusions extruding from the host SWNT. c) At 20 keV no significant interactions between Os and the SWNT take place on the timescale of our AC-HRTEM experiments; but there is some indication of carbon shell formation (top-left Os cluster) which would suggest that EBIR can persist even at 20 keV for this metal.

ways, determined by their positions in the periodic table. A high cohesive energy and the ability to form strong σ -bonds with carbon lead to substantial erosion of the carbon nanotube under an 80 keV electron beam, as observed in the case of Os. In contrast, a strong tendency to form metal–carbon π -bonds and metallic clusters with intermediate cohesive energy, as in the case of Ru, promotes the formation of new carbon nanostructures with the metal cluster acting as a template. The presence of a metal with highly stable metal carbide phases favors binding of the metal atoms within the carbide crystals, thus precluding any extensive interactions with the nanotube sidewall, as observed for Fe, but the resultant carbide is still able to facilitate the transformation of carbon into new nanostructures in AC-HRTEM experiments.

Because our methodology sheds light on the mechanisms of metal–nanocarbon interactions, these observations are relevant to any application of carbon nanotubes relying on the interface with transition metals, such as nanotube-based electronic devices. Our results suggest that a carbon nanotube is able to form strong σ -bonds with an electric contact made of Os and π -bonds with a Ru contact, whilst any interface with Fe is likely to transform into a layer of iron carbide. Considering the chemical similarities between SWNT and graphene, the same trend may apply to a graphene–metal interface. The exact atomic structure of the nanotube–metal interface determines the nature of the electron transport between the metal and the nanotube and thus defines the overall electronic characteristics of the device.

Another important implication of our AC-HRTEM observations is related to metal-catalyzed chemical transformations in carbon nanotubes. The electron beam in our experiments can be viewed as an “oxidizing agent”, such as O_2 , which in the presence of metal clusters removes carbon atoms from the nanotube sidewall via a series of complex transformations^[36] (e.g., etches the nanotube as if under oxidative conditions).^[37] Our comparative study of group VIII transition metals clearly indicates that the surface of Ru is readily passivated with carbon shells, and Fe transforms into carbide, and thus both of these metals become quickly deactivated, while Os remains

Table 2. Observed changes in the activity of Os clusters toward carbon nanotubes as a function of electron beam energy, and the amount of kinetic energy transferrable from the e-beam to carbon atoms.

	Electron beam energy		
	80 keV	40 keV	20 keV
Maximum transferrable kinetic energy from e-beam to carbon atom (T_{\max})	15.76 eV	7.59 eV	3.73 eV
EBIE activity	High	Low	Low
EBIR activity	Low	High	Medium

in its pure metallic form throughout the process. As carbon nanotubes are widely used as supports for metal-containing catalysts, our methodology provides valuable guidance for selecting particular types of metals for catalytic reactions.

Finally, our study has demonstrated for the first time that by controlling the energy of the e-beam (20–80 keV), we can drastically alter the pathways of chemical reactions of metals and effectively switch one type of reactivity to another. By reducing the e-beam energy from 80 to 40 keV EBIE changes to EBIR for Os, thus demonstrating the application of AC-HRTEM not only as a powerful imaging method but also as a new tool for controlling and studying chemical reactions. Another key outcome of these measurements is that the extent and rate of transformations promoted by the metal in SWNT decrease as a function of the kinetic energy transferred from the e-beam to carbon atoms (Table 2). This clearly emphasizes the fact that the reactions observed in nanotubes by AC-HRTEM are promoted primarily by the kinematic collisions of fast electrons of the e-beam with atoms (so-called *knock on* effects) rather than ionization or phonon excitation, the effects of which should increase as the energy of e-beam is decreased from 80 to 40 keV and to 20 keV. One of the reasons that knock on effects dominate in materials confined in nanotubes, and ionization and phonon excitation are less significant, is that SWNTs are excellent heat and electric conductors which effectively suppress any heating or ionization in the atoms and molecules confined in the nanotube under AC-HRTEM conditions.

4. Experimental Section

Electron Microscopy: HRTEM imaging was carried out using an image side C_s -corrected FEI Titan 80–300 transmission electron microscope operated at 80 kV acceleration voltage with a modified filament extraction voltage for information limit enhancement and an image side C_s -corrected Zeiss Libra 200MC TEM equipped with a monochromator (0.15 eV energy slit).^[38] This system was specially modified for low voltage operation and operated at 40 and 20 kV.^[39] Images were recorded either on a slow-scan CCD-camera type Gatan Ultrascan XP 1000 (FEI Titan) or a CMOS-camera type TVIPS 416T (Zeiss Libra). For all in situ irradiation experiments, the microscopes provided a highly controlled source of local and directed electron radiation on a selected area of the sample. Experimentally applied electron fluxes ranged from 2×10^6 to 9×10^6 e⁻ nm⁻² s⁻¹, and the total applied dose was kept the same, reaching $\approx 10^{10}$ e⁻ nm⁻² at the end of each experiment. TEM specimens were heated in air at 150 °C for 7 min shortly before

insertion into the TEM column. All imaging experiments were carried out at room temperature.

EDX spectra were recorded for small bundles of SWNTs (3–10 nanotubes) filled with each metal on a JEOL 2100F TEM equipped with an Oxford Instruments X-rays detector at 100 kV.

Image Simulation: TEM image simulation was carried out using the multislice program QSTEM. QSTEM uses the Dirac–Fock scattering potential of Rez et al.^[40] A fixed number of 30 slices per nanotube (corresponding to an average slice thickness of 0.05 nm) was chosen and images were calculated with a sampling of 0.015 nm per pixel. The aberration coefficients defocus parameters d_f , C_s , A_1 , and B_2 were set according to the imaging conditions in the specific experiment. The convergence angle was fixed at 0.5 mrad. A total focus-spread (standard deviation) σ_{df} of 4 nm was assumed, and direction sensitive vibrations with amplitudes in the order of 1 to 5 pm were included in the image simulation. The effect of limited electron dose was emulated by applying noise to the calculated images using a custom-made Monte-Carlo program exploiting the Poisson statistics of electrons. Atomic models of SWNTs were built using a custom-made program taking into account different chiralities, if determinable in the experimental images. The structural models of the clusters are based on scaled bulk structures, if the symmetry and zone axis could be determined. The complex models (clusters@SWNT) are rendered and iteratively fitted to the experimental results.

Materials Preparation: SWNT (arc discharge, NanoCarbLab) were annealed at 540 °C for 20 min to open their termini and remove any residual amorphous carbon from the internal cavities, a 20% weight loss was observed. For Ru and Os samples the metal carbonyl precursor, $Ru_3(CO)_{12}$ or $Os_3(CO)_{12}$ (10 mg) (used as supplied, Sigma Aldrich) was mixed with the SWNT (5 mg), sealed under vacuum (10^{-5} mbar) in a quartz ampoule and heated at a temperature slightly above the vaporization point of the respective metal carbonyl species for 3 d to ensure complete penetration of the SWNT by the metal carbonyl vapor. The sample was then allowed to cool. For Fe the SWNTs (5 mg) were immersed in a tetrahydrofuran (1 mL) solution of $Fe_3(CO)_{12}$ (10 mg) (Fisher Scientific) and stirred for 1 h under inert atmosphere. The solvent was removed by vacuum, fresh tetrahydrofuran (1 mL) added and the suspension stirred for a further 1 h. This process was repeated a total of three times. All samples were washed repetitively with tetrahydrofuran to remove any metal carbonyl from the exterior of the SWNT.

The nanotubes filled with metal carbonyls were sealed in a quartz ampoule under an argon atmosphere and heated at 600 °C, a temperature significantly above the decomposition point of the metal carbonyl species (≈ 150 – 200 °C), for 2 h to decompose the metal carbonyl into the desired pure metal nanoparticles. Alternatively the decomposition process can be achieved directly during TEM using the e-beam as the energy source. Metal particles formed by thermal and e-beam decomposition of the metal carbonyls are virtually indistinguishable.

Theoretical Modeling: Density functional theory was employed to perform the calculations for metal bonding with pristine (10, 10) SWNT and with different vacancies (single SV, double DV, and tetra TV) in the nanotube sidewall. The binding energy was calculated as E (binding energy) = E (SWNT + M) – E (SWNT) – E (M), where E (SWNT) is the nanotube energy, E (M) is the energy of an isolated metal atom and E (SWNT + M) is the energy of the structure containing the nanotube and metal atom.^[13]

The geometry optimization calculations of SV (10, 10) SWNT, DV (10, 10) SWNT, and TV (10, 10) SWNT structures were performed

with included spin polarization. Taking into account that CASTEP code changes the spin polarization to minimize the total energy of the system during the calculation, simulations with different initial spin polarization values were performed in order to confirm the final spin polarization. SV (10, 10) SWNT has the lowest energy with one unpaired electron (spin multiplicity = 2), DV (10, 10) SWNT with no unpaired electrons (spin multiplicity = 1), and TV (10, 10) SWNT with one unpaired electron (spin multiplicity = 2). These results were used in further calculations with different metals. Similarly, spin polarization was taken into account in metals interacting with pristine (10, 10) SWNTs and with different types of vacancies, as each metal (Fe, Ru, Os) has four unpaired electrons (spin multiplicity = 5). Trial calculations for M@SV (10, 10) SWNT, M@DV (10, 10) SWNT, and M@TV (10, 10) SWNT with different values of spin polarization were performed, and the calculated binding energies and charge transfer values for different metals and nanotubes are summarized in Table S1 in the Supporting Information.

Supporting Information

Supporting Information is available from the Wiley Online Library or from the author.

Acknowledgements

T.Z. and U.K. acknowledge the support of the "Graphene Flagship" and DFG SPP "Graphene". U.K., J.B., and T.Z. acknowledge the DFG and the Ministry of Science, Research and the Arts (MWK) of Baden-Wuerttemberg within the frame of the SALVE (Sub Angstrom Low-Voltage Electron Microscopy) project. E.B., T.W.C., and A.N.K. acknowledge ERC Consolidator Grants and EPSRC and NUST "MISiS" (grant K3-2015-030) for financial support, and Nottingham Nanotechnology and Nanoscience Centre (NNNC) for access to instrumentation. M.S. and E.B. are grateful to the High Performance Computing (HPC) Facility at the University of Nottingham for providing computational time. T.Z. and J.B. are grateful to Dr. G. Benner of Carl Zeiss company for assisting with the TEM experiments at 20 and 40 kV.

- [1] H. Valencia, A. Gil, G. Frapper, *J. Phys. Chem. C* **2010**, *114*, 14141.
- [2] K. T. Chan, J. B. Neaton, M. L. Cohen, *Phys. Rev. B* **2008**, *77*, 235430.
- [3] C. Inntam, J. Limtrakul, *J. Phys. Chem. C* **2010**, *114*, 1327.
- [4] S. H. Yang, W. H. Shin, J. W. Lee, S. Y. Kim, S. I. Woo, J. K. Kang, *J. Phys. Chem. B* **2006**, *110*, 13941.
- [5] H. Sevinçli, M. Topsakal, E. Durgun, S. Ciraci, *Phys. Rev. B* **2008**, *77*, 195434.
- [6] K. Kong, Y. Choi, B. Ryu, J. Lee, H. Chang, *Mater. Sci. Eng. C* **2006**, *26*, 1207.
- [7] Y. Ma, O. P. Lehtinen, A. S. Foster, R. M. Nieminen, *New J. Phys.* **2004**, *6*, 68.
- [8] N. Nemeč, D. Tománek, G. Cuniberti, *Phys. Rev. Lett.* **2006**, *96*, 076802.
- [9] G. Giovannetti, P. A. Khomyakov, G. Brocks, V. M. Karpan, *Phys. Rev. Lett.* **2008**, *101*, 026803.

- [10] H. L. Zhuanga, G. P. Zhenga, A. K. Sohb, *Comput. Mater. Sci.* **2008**, *43*, 823.
- [11] Y. K. Chen, L. V. Liu, W. Q. Tian, Y. A. Wang, *J. Phys. Chem. C* **2011**, *115*, 9306.
- [12] D. W. Boukhvalov, M. I. Katsnelson, *Appl. Phys. Lett.* **2009**, *95*, 023109.
- [13] A. V. Krasheninnikov, P. O. Lehtinen, A. S. Foster, P. Pyykkö, R. M. Nieminen, *Phys. Rev. Lett.* **2009**, *102*, 126807.
- [14] E. J. G. Santos, A. Ayuela, D. Sánchez-Portal, *New J. Phys.* **2010**, *12*, 053012.
- [15] J. A. Rodríguez-Manzo, O. Cretu, F. Banhart, *ACS Nano* **2010**, *4*, 3422.
- [16] Q. M. Ramasse, R. Zan, U. Bangert, D. W. Boukhvalov, Y. Son, K. S. Novoselov, *ACS Nano* **2012**, *6*, 4063.
- [17] Y. Zhang, N. W. Franklin, R. J. Chen, H. Dai, *Chem. Phys. Lett.* **2000**, *331*, 35.
- [18] Y. Gan, L. Sun, F. Banhart, *Small* **2008**, *4*, 587.
- [19] R. Zan, U. Bangert, Q. Ramasse, K. S. Novoselov, *Nano Lett.* **2011**, *11*, 1087.
- [20] R. Zan, U. Bangert, Q. Ramasse, K. S. Novoselov, *Small* **2011**, *7*, 2868.
- [21] F. Banhart, J.-C. Charlier, P. M. Ajayan, *Phys. Rev. Lett.* **2000**, *84*, 686.
- [22] N. P. E. Barry, A. J. Pitto-Barry, A. M. Sanchez, A. P. Dove, R. J. Procter, J. J. Soldevila-Barreda, N. Kirby, I. Hands-Portman, C. J. Smith, R. K. O'Reilly, R. Beanland, P. J. Sadler, *Nat. Commun.* **2014**, *5*, 3851.
- [23] J. C. Meyer, F. Eder, S. Kurasch, V. Skakalova, J. Kotakoski, H. J. Park, S. Roth, A. Chuvilin, S. Eyhuse, G. Benner, U. Kaiser, *Phys. Rev. Lett.* **2012**, *108*, 196102.
- [24] J. Kotakoski, A. V. Krasheninnikov, U. Kaiser, J. C. Meyer, *Phys. Rev. Lett.* **2011**, *106*, 105505.
- [25] Z. He, K. He, A. W. Robertson, A. I. Kirkland, D. Kim, J. Ihm, E. Yoon, G.-D. Lee, J. H. Warner, *Nano Lett.* **2014**, *14*, 3766.
- [26] T. Zoberbier, T. W. Chamberlain, J. Biskupek, N. Kuganathan, S. Eyhuse, E. Bichoutskaia, U. Kaiser, A. N. Khlobystov, *J. Am. Chem. Soc.* **2012**, *134*, 3073.
- [27] F. Banhart, *Nanoscale* **2009**, *1*, 201.
- [28] P. Serp, B. Machado, *Nanostructured Carbon Materials for Catalysis*, RSC Catalysis Series No. 23, Royal Society of Chemistry, Cambridge, UK, **2015**.
- [29] A. Chuvilin, A. N. Khlobystov, D. Oberfell, M. Haluska, S. Yang, S. Roth, U. Kaiser, *Angew. Chem., Int. Ed.* **2010**, *49*, 193.
- [30] B. W. Smith, D. E. Luzzi, *J. Appl. Phys.* **2001**, *90*, 3509.
- [31] T. W. Chamberlain, T. Zoberbier, J. Biskupek, A. Botos, U. Kaiser, A. N. Khlobystov, *Chem. Sci.* **2012**, *3*, 1919.
- [32] M. A. Turchanin, P. G. Agraval, *Powder Metall. Met. Cer.* **2008**, *47*, 26.
- [33] *Moffatt's Handbook of Binary Phase Diagrams*. (Ed. J. H. Westbrook), Genium Publishing Corporation: New York, **1992**.
- [34] H. Amara, C. Bichara, F. Ducastelle, *Phys. Rev. Lett.* **2008**, *100*, 056105.
- [35] T. W. Chamberlain, J. C. Meyer, J. Biskupek, J. Leschner, N. B. Besley, E. Bichoutskaia, U. Kaiser, A. N. Khlobystov, *Nat. Chem.* **2011**, *3*, 732.
- [36] I. V. Lebedeva, T. W. Chamberlain, A. M. Popov, A. A. Knizhnik, T. Zoberbier, J. Biskupek, U. Kaiser, A. N. Khlobystov, *Nanoscale* **2014**, *6*, 14877.
- [37] N. Severin, S. Kirstein, I. M. Sokolov, J. P. Rabe, *Nano Lett.* **2009**, *9*, 457.
- [38] J. Biskupek, P. Hartel, M. Haider, U. Kaiser, *Ultramicroscopy* **2012**, *116*, 1.
- [39] U. Kaiser, J. Biskupek, J. C. Meyer, J. Leschner, J. Lechner, H. Rose, M. Stöger-Pollach, A. N. Khlobystov, P. Hartel, P. U. Kaiser, *Ultramicroscopy* **2011**, *111*, 1239.
- [40] D. Rez, P. Rez, I. Grant, *Acta Crystallogr.* **1994**, *A50*, 481.

Received: July 24, 2015
Revised: November 19, 2015
Published online: February 5, 2016